MNRAS **000**, 000–000 (0000) Preprint 20 January 2022 Compiled using MNRAS LATEX style file v3.0

WR-BH systems compose 90% of the Gravitational Wave mergers of Binary Black Holes at $Z = 0.02$ and $Z = 0.002$

Erika Korb,[1]
[1] *Physics and Astronomy Department Galileo Galilei, University of Padova, Vicolo dell'Osservatorio 3, I-35122, Padova, Italy*

20 January 2022

ABSTRACT

We used the SEVN2 population synthesis code to analyze the formation and evolution of systems composed by a Wolf Rayet and a Black Hole (WR-BH) in the isolated binary scenario. We aim to put constraints on their role in the formation of the Binary Black Holes (BBHs) that merge via Gravitational Wave emission within a Hubble time (GW-BBHs). We simulated four sets of $\sim 10^6$ binaries exploring a four-dimensional parameter of space, composed of two metallicities $Z = 0.02$ and $Z = 0.002$ and two Core-Collapse SuperNova models implemented in SEVN2, delayed and compact. In each set we find that more than $\sim 90\%$ of the formed GW-BBHs have evolved through the WR-BH configuration, although WR-BH systems composed only $\sim 1 - 15\%$ of all the simulated systems. At $Z = 0.02$, about $\sim 24 - 59\%$ of the WR-BH systems that formed a GW-BBH came from binaries where one of the object had more than the 80% of its Roche Lobe filled. At $Z = 0.002$ we find that this percentage drops to $\sim 0.4-7\%$. This metallicities favour the formation of GW-BBHs, which have remnants with $3\ M_\odot \lesssim M_{\rm rem} \lesssim 30 M_\odot$ and progenitors with $20\ M_\odot \lesssim M_{\rm ZAMS} \lesssim 80 M_\odot$. On the contrary, at $Z = 0.02$ we obtained less GW-BBHs systems. They exhibit remnants with $3\ M_\odot \lesssim M_{\rm rem} \lesssim 20 M_\odot$ and progenitors with $20\ M_\odot \lesssim M_{\rm ZAMS} \lesssim 60 M_\odot$.

1 INTRODUCTION

The detection of the first Gravitational Wave (GW) GW150914 (Abbott et al. (2016)) not only confirmed the existence of Binary systems made of two stellar Black Holes (BBHs) but also demonstrated that such systems are capable of merging via emission of GWs within a Hubble time H_0 (hereafter we will call such systems GW-BBHs for brevity). Since then, the gravitational wave detectors of the LIGO Scientific, Virgo and KAGRA (LVK) Collaboration discovered ~ 80 GW-BBHs, as reported in the third Gravitational-Wave Transient Catalog (GWTC-3), recently published by The LIGO Scientific Collaboration & et al. (2021).

Abbott et al. (2021b) and Fishbach & Kalogera (2021) analyzed the remnant properties of the GWTC-2 catalogue (Abbott et al. (2021a)) and concluded that such systems could both evolve from isolated binaries in the galactic field and from dynamically active environments, such as young star clusters. The observations revealed merging BBHs with very different combinations of masses and spins, providing a precious sample to test and perfectionate the aforementioned models. In fact, in the first scenario, we expect that the evolution is dominated by binary processes like the Common Envelope (CE) and the Roche Lobe Overflow (RLO), that favour the sharing of mass and angular momentum between the two components and the production of remnants with aligned spins (Kalogera (2000)) and similar masses, up to $\sim 50\ M_\odot$ (Giacobbo et al. (2018)). In the second scenario we expect that hierarchical mergers and binary exchanges allow the formation of BHs in the pair-instability gap ($\sim 60 - 120\ M_\odot$), with mass ratios $q = M_2/M_1$ far from unity (Rastello et al. (2021)) and misaligned spins (Rodriguez et al. (2016)).

From an observational point of view, BBHs progenitors can be searched in binary systems that already contain a stellar BH. Nevertheless, BHs in quiescent systems are very difficult to observe with radial velocity (Thompson et al. (2019)) and astrometric measurements (Wyrzykowski & Mandel (2020)) and hopefully the new Gaia Data Releases will shade more light on them. On the contrary, BHs can be visible in the X-ray band if they are accreting mass from a companion star. These systems are called Black Hole X-Ray Binaries (BH-XRBs) and, according to Fishbach & Kalogera (2021), their progenitors share the same mass distribution of the progenitors of the primary BHs in the GWTC-2 catalogue (although the GW-BBHs progenitors exhibit slower spins, which leaves the debate open).

In this paper we will focus on the BH-XRBs systems made up by a Wolf-Rayet (WR) and a BH (hereafter, WR-BH systems) and we will try to constrain the conditions under which they could be progenitors of GW-BBHs systems in the isolated binary evolution scenario. We expect that these are very good candidates to form a GW-BBH, given that at solar metallicity $Z = Z_\odot = 0.02$ the WRs are formed from stars with initial mass $M_{\rm ZAMS} \gtrsim 30\ M_\odot$ (Limongi & Chieffi (2010)), have strong line-driven winds and high mass loss rates $\dot{M} \sim 10^{-4} - 10^{-5}\ M_\odot/{\rm yr}$ (Gräfener & Hamann (2008)). This means that WR stars are more likely to form a secondary BH in the neutrino-driven SuperNova (SN) sce-

Host galaxy	Name	BH mass [$M_\odot$]	WR mass [$M_\odot$]	Period [h]	$t_{\rm GW}$ [Gyr]	Z [$Z_\odot$]
IC 10	IC10 X-1	23-33[a]	35[b]	34.9[a]	3.5	0.22
NGC 300	NGC300 X-1	13-21[d]	26[c]	32.8[d]	2.9	0.19
M101	M101 ULX-1	20-30	19	196.8	348	0.17
Milky Way	Cyg X-3	3	7	4.8	0.017	0.31
NGC 4490	CXOU J123030.3+413853	-	-	6.4	0.038	0.23
NGC 253	CXOU J004732.0-251722.1	-	-	14.5	0.33	0.24
Circinus	CG X-1	-	-	7.2	0.051	0.10

[a] Silverman & Filippenko (2008) [b] Clark & Crowther (2004) [c] Crowther et al. (2010) [d] Binder et al. (2021)

Table 1. Properties of the seven WR-BH candidates. The table is inspired by Esposito et al. (2015). $t_{\rm GW}$ is an order-of-magnitude estimate calculated assuming $M_{1,\rm BH} = M_{2,\rm BH} = 10\ M_\odot$, given the uncertainties in the mass determination discussed in Section 2. The other parameters are extracted from the above referenced papers and from Liu et al. (2013) (M101 ULX-1), Zdziarski et al. (2013) (Cyg X-3), Esposito et al. (2013) (CXOU J123030.3+413853), Maccarone et al. (2014) (CXOU J004732.0-251722.1), Esposito et al. (2015) (CG-X1), Mapelli et al. (2010) (Z).

nario (threshold at $M_{\rm ZAMS} \gtrsim 25\ M_\odot$ for BH formation, Sukhbold et al. (2016)), and to produce a bright accretion disk around the primary BH ($L_{\rm X} \gtrsim 10^{36}$ erg/s, Tutukov et al. (2013)).

In Section 2 we will review the seven WR-BH candidates, discussing their uncertainties. In Section 3 we will describe the properties of the SEVN2 code that we used and in Section 4 we will illustrate the initial conditions that we adopted. In Section 5 we will present and discuss the results of the simulations, summing up the main points in Section 6.

2 OBSERVED WR-BH SYSTEMS

In the Table 1 we report the seven WR-BH candidates and their discovery papers, although the WR/BH nature of the objects and their properties are still a matter of debate.

On one hand, spectroscopic observations confirmed the existence of a WR in IC10 X-1, NGC300 X-1, M101 ULX-1 and Cyg X-3 (see the papers in the Table 1). On the other hand, Tutukov et al. (2013) and Laycock et al. (2015) pointed out the dynamical mass measurements of the BHs of IC10 X-1 and NGC300 X-1 need to be revised because the orbital period derived from spectroscopy was not in phase with the X-ray light curve. For instance, Binder et al. (2021) recently derived a more reliable estimate for the BH mass of NGC300 X-1 using the C IV λ1550 line in place of the commonly used He II λ4686 line, that was not tracing the orbital motion of the WR. Even though this line is probably related to hot spots in the accretion disk generated by the accretion stream, we notice that Binder et al. (2021) found a $M_{\rm BH} \sim 13 - 21\ M_\odot$ estimate close to the one of $M_{\rm BH} \sim 14 - 20\ M_\odot$ obtained by Crowther et al. (2010) with the He II λ4686 line. Thus it is probable that also the BH masses of IC10 X-1 and M101 ULX X-1 are in the correct mass range, even though they have been estimated with the He II λ4686 line so they need to be revised.

The uncertainty in the compact object of Cyg X-3 lies in its physical interpretation. In fact, its mass is close to the maximum allowed mass of $\sim 3\ M_\odot$ required by the equation of state of a NS (Kalogera & Baym (1996), Alsing et al. (2018)). Thus Cyg X-3 could host a BH or a NS, even tough the BH nature seems to be favoured by radio, infrared and X-ray emissions (Zdziarski et al. (2013)).

The last three systems (CXOU J123030.3+413853, CXOU J004732.0-251722.1 and CG X-1) are WR-BH candidates only on the basis on X-ray measurments. In fact, Esposito et al. (2013); Esposito et al. (2015); Maccarone et al. (2014), interpret the slow rises and fast decays of the X-ray light curve with regions of stronger and lighter interaction between the ionized matter of the WR winds and the X-radiation. The authors base their reasoning on a parallelism with the interpretation of the light curve modulations of Cyg X-3, that is known to host a WR and a compact object (Hertz et al. (1978); Zdziarski et al. (2010); van Kerkwijk et al. (1996)).

Even though the masses and the nature of the compact objects are quite uncertatin, we can still compute an oder-of-magnitude estimate for the time needed for the resulting compact object binary to merge via GW emission $t_{\rm GW}$ using the Peters (1964) formula:

$$t_{\rm GW} = \frac{5}{256} \frac{c^5 a^4 (1-e^2)^{7/2}}{G^3 M_1 M_2 (M_1 + M_2)} \quad (1)$$

where G is the gravitational constant, c is the speed of light and a is the semi-major axis. Similarly to what Esposito et al. (2015) propose, we assume: a circular orbit (eccentricity $e = 0$), a secondary BH of $M_{2,\rm BH} \sim 10\ M_\odot$ produced by the WR and also a primary BH of $M_{1,\rm BH} \sim 10\ M_\odot$. Such masses are probably smaller than the real ones but it allows us to obtain an upper boundary for $t_{\rm GW}$. With these assumptions we find that a binary needs to have a period $P \lesssim 10$ days ($a \lesssim 20\ R_\odot$) in order to merge within a Hubble time. By comparing this value with the ones reported in the Table 1, we conclude that binary systems that formed with characteristics similar to the WR-BH candidates could produce a GW-BBHs observable today (except systems like M101 ULX X-1, too wide to merge within a Hubble time).

3 POPULATION SYNTHESIS WITH THE SEVN2 CODE

3.1 Overview of the SEVN2 code

SEVN2 is the implementation of the Stellar EVolution for N-body simulations (SEVN) code described in Spera et al. (2015), Spera & Mapelli (2017) and Spera et al. (2019). Written entirely in `C++`, SEVN2 is a fast and flexible population synthesis code that evolves the stars by reading a set

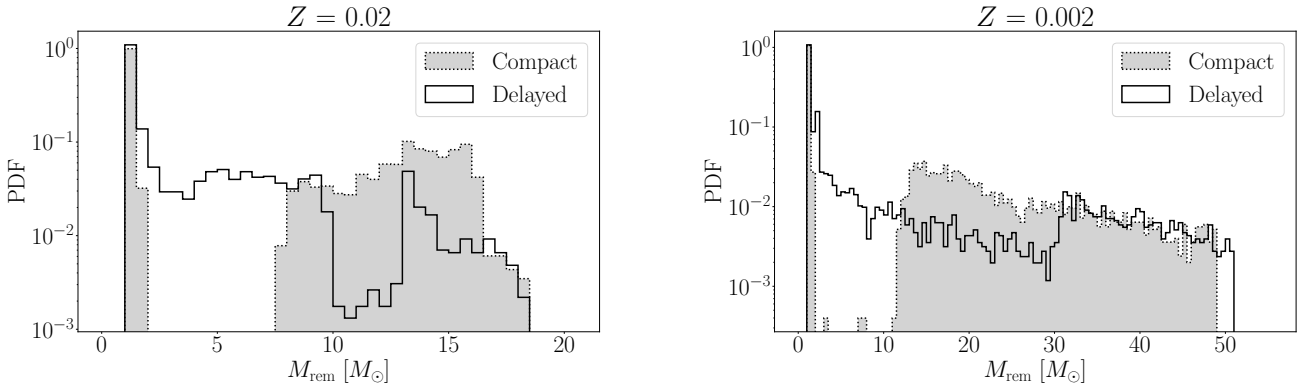

Figure 1. BH and NS mass distribution obtained from stars with different metallicities $Z = 0.02$ and $Z = 0.002$ and different SN prescription: delayed (Fryer et al. (2012), Spera et al. (2015)) and compact (O'Connor & Ott (2011), Mapelli et al. (2020)).

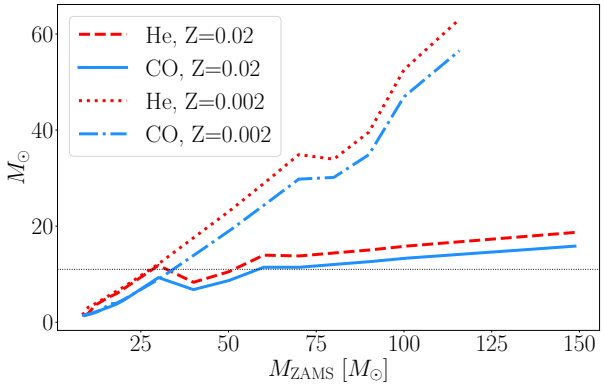

Figure 2. Helium and Carbon-Oxygen core mass at the end of the pre-SN stage as a function of the initial star mass $M_{\rm ZAMS}$. The limit of $M_{\rm CO} = 11\ M_\odot$ is marked with a black dotted line.

of tabulated stellar evolutionary tracks and interpolating on-the-fly their physical parameters. Thus, SEVN2 can be esily implemented to adopt the most updated models for stellar evolution just by adding the new pre-computed tracks to the SEVN2 database.

SEVN2 evolves the "real" star as a collection of time-steps of a "fake" star, that at each time-step is interpolated by weighting the four tabulated evolutionary tracks with the closest value of mass M and metallicity Z. The code ensures that at each time-step both the "fake" star and the interpolating tracks are in the same phase (e.g. 10% of the He-burning phase). SEVN2 matches this condition also when it needs to search for new interpolating tracks for stars that changed their properties above a given threshold, for instance because they accreted mass, their enveolpe was strippped or they collided with the companion.

The code implements an adaptive time-step scheme to account for different timescales in the different evolutionary stages.

3.2 WR stars, He-stars and stellar winds

When the Helium core achieves the 98% of the total stellar mass, the star is considered as a WR[1]. Its evolution is interpolated from He-stars tracks i.e. usual H-stars from which the H envelope was removed at the onset of the He-burning (therefore maintaining the chemical composition of the original star).

WR stars are usually O-type stars that evolved close to the Humphrey-Davidson limit (Humphreys & Davidson (1979)) i.e. close to the Eddington limit $\Gamma_e \sim 1$, where $\Gamma_e = L/L_e$ quantifies how much the luminosity L of the star is close to the maximum luminosity L_e that the star can hold not to disrupt under the radiation pressure. Stars in this region rapidly evolve into the Luminous Blue Variable (LBV), Blue Super Giant (BSG) or Red Super Giant (RSG) stages, eventually becoming a WR.

SEVN2 adopts the `PARSEC` evolutionary tracks developed by Chen et al. (2015), which calculate the mass-loss rates as follows: stars in the BSG, RSG and LBV phase implement the mass loss rates of Gräfener & Hamann (2008), that are proportional to the metallicity Z and depend on the Eddington parameter Γ_e, while WR stars have mass-loss rates that are proportional also on their helium mass fraction Y and luminosity L, as found by Nugis & Lamers (2000).

A we can see in Figure 1 and 2, the higher the metallicity Z, the stronger the line-driven winds and the lighter the remnants. Even though the remnant masses strongly depend on the SN prescription (see the next section), on average we expect maximum remnant masses of ~ 20 for $Z = 0.02$ and of ~ 50 for $Z = 0.002$ (i.e. before entering the pair-instability regime).

3.3 Prescriptions for SuperNovae (SNe)

SEVN2 implements five types of Core-Collapse SNe (CC-SNe) and includes also treatments for Pair-Instability SNe and Pulsational Pair-Instability SNe, as described in Spera et al. (2015), Spera & Mapelli (2017), Spera et al. (2019) and

[1] In coding terms, the WR star is identified with the phase $k = 7, 8, 9$ as in the Table 1 of Spera et al. (2019).

Mapelli et al. (2020). Given that the SN explosion is a rather complex mechanism, each description tries to parametrize the general behaviour but stil provides a rough treatment.

In this paper we will try to obtain results that are independent on the model of CCSN that we choose, therefore we will repeat our simulations adopting first the delayed model of Fryer et al. (2012) and then the compactness criterion of O'Connor & Ott (2011), hereafter called compact model. The models are implemented as described respectively in Spera et al. (2015) and Mapelli et al. (2020). As it is clearly visible in Figure 1, for a fixed metallicity the different SN models result in very different mass distributions of the compact remnants $M_{\rm rem}$ (NS and BH).

On the one hand, the delayed model considers direct collapses for stars with large CO core mass at end of the pre-SN stage, i.e. for $M_{\rm CO} > 11\ M_\odot$. Stars below this threshold explode and accrete only a fraction $f_{\rm fb}$ (fallback) of the ejected envelope mass. Fryer et al. (2012) set both the mass of the proto-compact object and the fallback f_b proportional to the $M_{\rm CO}$, therefore the $M_{\rm rem}$ distribution strongly mimics the $M_{\rm CO}$ distribution. Thus, when massive stars suffer winds that limit their core growth, we find a lower production of BH in the correspondent mass range. From the Figure 2 we can see that this depletion affects stars with $30\ M_\odot \lesssim M_{\rm ZAMS} \lesssim 60\ M_\odot$ and $60\ M_\odot \lesssim M_{\rm ZAMS} \lesssim 100\ M_\odot$ and results in a lower number of BH with $10\ M_\odot \lesssim M_{\rm BH} \lesssim 13\ M_\odot$ and $20\ M_\odot \lesssim M_{\rm BH} \lesssim 30\ M_\odot$, for $Z = 0.02$ and $Z = 0.002$ respectively. For stars with $M_{\rm ZAMS}$ outside these intervals, the winds don't limit so much the mass of the core, that instead grows linearly with the $M_{\rm ZAMS}$ and produces BHs with masses proportional to it, as visible in Figure 1.

Similarly to the delayed model, also the compactness criterion of O'Connor & Ott (2011) $\xi_{2.5}$ (that measures the radius that encloses $2.5 M_\odot$ bayonic masses at the core bounce) is implemented in SEVN2 as a function of the $M_{\rm CO}$, following Mapelli et al. (2020):

$$\xi_{2.5} = \frac{2.5/M_\odot}{R(2.5)/1000\ \rm km} = 0.55 - 1.1(M_{\rm CO}/M_\odot)^{-1} \qquad (2)$$

Sukhbold & Woosley (2014) and Sukhbold et al. (2016) showed that the $\xi_{2.5}$ is not a monotonic function of the $M_{\rm CO}$ so Mapelli et al. (2020) accounted for it using a stochastic explosion/implosion decision method following the distributions described in Patton & Sukhbold (2020). Thus, stars that explode will form a NS while stars that directly collapse will form a BH, whose mass is proportional to the Helium core mass $M_{\rm He}$ at the end of the pre-SN stage and still implements a fallback parameter f_H, calibrated at $f_H = 0.9$ (see Mapelli et al. (2020) for more details). This mechanism allows the compact model to form BHs from stars with $M_{\rm ZAMS} \gtrsim 13\ M_\odot$, wherease the delayed model allowed only stars with $M_{\rm ZAMS} \gtrsim 20\ M_\odot$. These lower limits for the progenitors are valid both for $Z = 0.02$ and $Z = 0.002$.

The randomicity introduced in the explodability avoids the creation of the "factitious dips" discussed in the delayed model and produces $M_{\rm rem}$ with a distribution that mimics the one of the $M_{\rm ZAMS}$. On the contrary, this model favours the explosion of stars with masses $M_{\rm ZAMS} \lesssim 20 M_\odot$ (Sukhbold et al. (2016)), producing a gap in $M_{\rm rem} \sim 2 - 7(10)\ M_\odot$ for $Z = 0.02(0.002)$ that seems in agreement with the well-known $2 - 5\ M_\odot$ mass gap, observed both in X-ray binaries (Özel et al. (2010)) and in GW-BBHs (The LIGO Scientific Collaboration & et al. (2021)).

When the SN occurs, the remnant receives a kick that can unbound the system. SEVN2 draws a random kick from the Maxwellian distribution of Hobbs et al. (2005) and scales it with the fallback $f_{\rm fb}$ already used in the delayed model, as described in Spera et al. (2015).

If the system survives the SN kicks and forms a binary of compact objects, SEVN2 adopts the Equation 1 to compute the time needed for system to merge via GW emission.

3.4 Prescriptions for binary evolution

SEVN2 implements the Hurley et al. (2002) prescriptions for the binary evolution, with some modifications, as described in detail in Spera et al. (2015, 2019).

We recall that, according to the Bondi & Hoyle (1944) spherical accretion formalism implemented, wind fed systems experience an inefficient mass transfer where the secondary accretes only $\sim 1 - 10\%$ of the mass lost by the primary. More efficient accretion rates occur during stable RLO events, where the mass is channelled towards the secondary and the transfer can be stable up to thermal timescales (Eggleton (1983); Webbink (1985)).

If the RLO is unstable on a dynamical timescale, both stars fill their Roche Lobe or a collision occurs, SEVN2 triggers a CE event. The code checks the type of stars entering the CE and directly merges the stars if the donor has not yet started the He-burning phase i.e. lacks of a well-developed core to survive to the envelope stripping. In the other cases, SEVN2 enters the routine to compute if the system will survive to the CE and with which parameters. The code implements the $\alpha\lambda$ formalism of Webbink (1984) to parametrize with α the fraction of orbital energy needed to expell the envelope and with λ the binding energy of the common envelope. The semi-major axis of the system at the end of the CE phase, therefore the survival of the system, is a function of these parameters and provides one of the main sources of uncertainties in the simulations along with the SN model. In our simulations we will follow Giacobbo et al. (2018), adopting $\alpha = 5$ and deriving λ from the polynomial fitting-formulae obtained by Claeys et al. (2014) on different stellar types .

4 INITIAL CONDITIONS

We used the `IC4popsyn` package developed by Nicola Giacobbo[2] to generate the initial set of binaries adopting the formalism required by the SEVN2 input.

First we generated the masses of the primary stars M_1 following the Kroupa (2001) Initial Mass Function (IMF):

$$\xi(M_1) \propto M_1^{-2.3} \qquad M_1 \in [10, 150]\ M_\odot \qquad (3)$$

We chose the lower boundary of $M_{1,\rm min} = 10\ M_\odot$ as a compromise between the need to simulate stars with $M_{\rm ZAMS} \lesssim 25\ M_\odot$, able to accrete mass from the companion

[2] `https://github.com/GiacobboNicola/IC4popsyn`

and form a BH, and the need to obtain secondaries with values included in the PARSEC tables, i.e. $M_2 > 2.2\ M_\odot$.

In fact, the distribution of the masses of the secondaries $\xi(M_2)$ is obtained from the primary distribution $\xi(M_1)$ and the mass ratio distribution $\xi(q)$, with $q = M_2/M_1$. We adopted the Sana et al. (2012) distribution, derived from binaries containing O-type stars sampled in six Galactic open clusters, so we obtained:

$$\xi(q) \propto q^{0.1} \qquad q \in [0.1, 1] \tag{4}$$

$$\xi(M_2) = \xi(M_1) \cdot \xi(q) \qquad M_2 \in [1\ M_\odot, M_1] \tag{5}$$

Similarly to before, the minimum value $q_{\rm min} = 0.1$ was a calibrated compromise that allows to explore all the reasonable mass combinations without producing too many secondaries below the PARSEC tables threshold of $M_2 > 2.2\ M_\odot$. In this case, the $M_{1,\rm min} = 10\ M_\odot$ results in a $M_{2,\rm min} = 1 < 2.2\ M_\odot$ therefore we had to generate $1.15 \cdot 10^6$ binaries in order to simulate $\sim 1.09 \cdot 10^6$ systems. Nevertheless, the $\sim 6 \cdot 10^4$ systems not simulated won't affect our conclusions, since masses so low wouldn't have produced a BH and wouldn't have resulted in a BBH under any circumstance.

We also generated the orbital periods P adopting the Sana et al. (2012) distribution for the logarithimc orbital periods $\mathcal{P} = \log(P/\text{days})$:

$$\xi(\mathcal{P}) \propto \mathcal{P}^{-0.55} \qquad \mathcal{P} \in [0.30, 5.5] \tag{6}$$

We followed the Moe & Di Stefano (2017) prescriptions and set $P = 2$ days ($\mathcal{P} = \log(P = 2) = 0.3$) as the lower limit for the period distribution, assuming that binaries with shorter period already circularized. In fact, Moe & Di Stefano (2017) showed that there is a complex correlation between the mass ratio q, period P and eccentricity e of early-type binaries containing O-type and B-type main sequence stars. Even though we assumed that q and P distributions are independent for simplicity, we try to account for it correlating P and e following their suggested prescription:

$$\xi(e(P)) \propto 1 - (P/\text{days})^{-2/3} \qquad P \geq 2 \text{ days} \tag{7}$$

As previously mentioned, we will adopt both the delayed and compact model for CCSNe. For the binary evolution we choose $\alpha = 5$ and λ according to Claeys et al. (2014).

5 RESULTS AND DISCUSSION

We ran four sets of $\sim 10^6$ binaries each, testing the metallicities solar $Z = Z_\odot = 0.02$ and sub-solar $Z = 0.002$ with both the delayed and compact model for CCSNe. The results are reported in the Tables 2, 3, 4, 5. Each table refers to binaries with different properties: in Table 2 we collect data from all the simulated binaries; in Table 3 only binaries that form a WR-BH system are counted; in Table 4 and 5 we restrict only to WR-BH systems that, while in that configuration, contain an object that fills its Roche Lobe (RL) more than 80% and 100%, respectively. For more information on the definition and properties of Table 4 and 5 see Section 5.2.2.

	$Z = 0.02$		$Z = 0.002$	
SN model	delayed	compact	delayed	compact
Simulated	1 090 704	1 090 733	1 091 005	1 069 343
BBH	78 476	104 228	101 137	165 750
bBBH	26 228	94 812	71 650	156 022
GW-BBH	47	237	9 540	23 411

Table 2. All binaries.

	$Z = 0.02$		$Z = 0.002$	
SN model	delayed	compact	delayed	compact
WR-BH	14 536	42 837	87 467	165 782
to BBH	6 448	15 969	45 933	90 898
to bBBH	3 918	15 969	43 354	90 858
to GW-BBH	46	212	9 538	23 397

Table 3. Only binaries that formed a WR-BH system.

	$Z = 0.02$		$Z = 0.002$	
SN model	delayed	compact	delayed	compact
WR-BH 80% fill	735	9 095	12 570	31 289
to BBH	11	155	35	1 730
to bBBH	11	155	35	1 730
to GW-BBH	11	152	35	1 730

Table 4. Wind fed WR-BH binaries that filled 80% of their RL.

	$Z = 0.02$		$Z = 0.002$	
SN model	delayed	compact	delayed	compact
WR-BH RLO	629	8593	11 363	27 753
to BBH	2	102	11	428
to bBBH	2	102	11	428
to GW-BBH	2	102	11	428

Table 5. WR-BH that experienced a RLO or a CE, filling completely their RL.

For each binary type, i.e. within each table, we restricted our analyisis to the following categories: all simulated binaries of that kind, binaries that form a BBH, binaries that form a bound BBH (labelled with bBBH for brevity) and binaries that form a GW-BBH.

5.1 GW-BBHs made by WR-BH systems

In Table 6 we computed how many WR-BH formed in each category with respect to the total number of binaries that fell in that category i.e. we took the ratio between Table 3 and 2. Even though only 1-15% of the simulated binaries will produce a WR-BH system, these binaries will made up more than 90% of all the BBHs that can merge via GW emission within a Hubble time. Moreover, Table 4 and 5 suggests that the WR-BH systems that fill their RL more than 80% and collapse into a BBH system are destined to form a GW-BBHs. We can draw similar considerations for WR-BH systems that overfill their RL by comparing Table 4 and 5. All these results seem to be independent on the metallicity and the SN model chosen.

At lower metallicities the WR-BH systems are more

	$Z = 0.02$		$Z = 0.002$	
SN model	delayed	compact	delayed	compact
to total	1%	4%	8%	16%
to BBH	1%	15%	45%	55%
to bBBH	15%	17%	61%	58%
to GW-BBH	98%	90%	99%	99%

Table 6. Percentage of WR-BH systems that satify a given a condition with respect to all the simulated systems that satisfy the same condition (see Section 5 for further details).

	$Z = 0.02$		$Z = 0.002$	
SN model	delayed	compact	delayed	compact
BBH/total	44%	37%	53%	54%
bBBH/BBH	61%	100%	94%	99%
GW-BBH/bBBH	1%	1%	22%	25%

Table 7. Relative importance of each subset of WR-BH with respect to the nearest larger set.

	$Z = 0.02$		$Z = 0.002$	
SN model	delayed	compact	delayed	compact
80% fill/WR-BH	5%	21%	14%	19%
BBH/80% fill	0.2%	1%	0.08%	2%
bBBH ratio	0.3%	1%	0.08%	2%
GW-BBH ratio	24%	59%	0.4%	7%

Table 8. Frequencies of each 80% WR-BH filling binaries property compared with the corresponding WR-BH property.

common in the stages prior to the GW merging. This could be due to the fact that lower metallicity means weaker stellar winds (see Section 3.2). If massive stars are able lose slowly their envelope it means that they will become WR late enough for the primary star to have already collapsed into a BH. On the contrary, for high metallicities the envelope is rapidly stripped and the WR may form and collapse into a BH before the primary does it. In this case, it could still be possible to form a BBH system, but it won't be a system that went through a WR-BH configuration (thus, the lower counts at $Z = 0.02$). We underline that this resoning is more likely for systems that undergo strong mass transfer episodes and that therefore accelerate or decelerate the stages of the star evolution, with the possibility that the role of the two stars is swapped.

We also find that the compact SN model favours the formation of WR-BH systems with respect to the delayed SN model. This could be related to the fact that the compact model allows the formation of BHs from stars with $M_{\rm ZAMS} \gtrsim 13\ M_\odot$, while the delayed model has an higher lower boundary of $M_{\rm ZAMS} \gtrsim 20\ M_\odot$ (see Section 3.3). Thus, we expect that the compact model forms more BHs, increasing the probability that some of these will be part of a system containing a WR.

It is likely that the extra production of WR-BH systems from the compact model falls in the region of parameter space that influences the RL filling properties of the binary. From Table 8 we notice that not only higher metallicities result in a higher percentage of GW-BBHs that filled their RL more than 80%, but also that with the compact model this percentage rises to $\sim 60\%$, more than twice with respect to the $\sim 24\%$ found with the delayed model.

In Table 7 we see that only $\sim 50\%$ of the WR-BHs will form a BBH and only $\sim 25\%$ of such BBHs will form a GW-BBH at $Z = 0.002$ (the percentages are even lower for $Z = 0.02$). Nevertheless, WR-BHs seem to form mainly bound BBHs, either because BHs have small SN kicks (see Section 3.3) or because the objects are already in a close orbit. In Section 5.2.2 we will see that the GW-BBHs systems experienced one or two CE phases, so the last hypothesis could be plausible also for the BBHs that don't merge but are still bound. Nevertheless, these considerations allow us to discuss only the bound BBH systems in place of all the BBH systems without losing generality.

5.2 Progenitors and remnants mass distributions

Hereafter we will label as primary M_1 and secondary M_2 stars the objects that were, respectively, more and less massive in the progenitor system.

In Figure 3 we report the mass distribution of progenitors and remnants for the primary star for WR-BH systems that formed a bound BBH and possibly a GW-BBH. For brevity we omitted the distribution for the secondaries, given that it shares the same features of Figure 3 with the exception of the upper boundary of progenitor mass allowed to form bound BBH systems that evolved with the delayed model at $Z = 0.02$, that is $\sim 70\ M_\odot$. Nevertheless, we can explore the evolution of the secondaries by looking at Figure 5 that, along with Figure 4 for the primaries, compares the progenitor masses with the correspondent remnant masses.

In Figure 3 we notice that the progenitor distribution of the bound BBH systems with $Z = 0.002$ deviates from the generated power law distribution (see Section 4) for $20M_\odot \lesssim M_{\rm ZAMS} \lesssim 80M_\odot$, regardless of the SN model adopted. Deviations are present also at $Z = 0.02$, even though, when the delayed model is implemented, they are stronger and limited to the $20M_\odot \lesssim M_{\rm ZAMS} \lesssim 60M_\odot$ range. We notice that these ranges coincides, roughly speaking, with the masses of the progenitors for the GW-BBHs systems. By looking at Figure 4 and 5 we notice that these binaries produce indeed the majority of bound BBH and GW-BBH systems. Thus, progenitors in these mass ranges for the given metallicities will likely form WR-BH systems that form a bBBH merging via GW emission within a Hubble time.

We further notice that the range of interest at $Z = 0.02$ coincides with the one affected by stellar winds that limit the growth of the CO core and the remnant mass (see Section 3.3). The delayed model is strongly dependent of the CO mass and exactly for these masses favours the production of BHs lighter than expected . We think that such BHs are so light ($M_{\rm BH} \lesssim 10\ M_\odot$) that they are easily kicked out from the binary when they form. This overproduction of light BHs in future broken systems is likely more frequent than the production of BHs in bound BBHs (possibly GW-merging) and could explain the lower number of bBBHs produced by $20M_\odot \lesssim M_{\rm ZAMS} \lesssim 60M_\odot$ progenitors. In fact, in the same mass range and metallicity, the distribution obtained from the compact model doesn't exhibit a decrease in the number of counts so strong. Moreover, the same effect of the delayed model is much less important and visible in the $Z = 0.002$

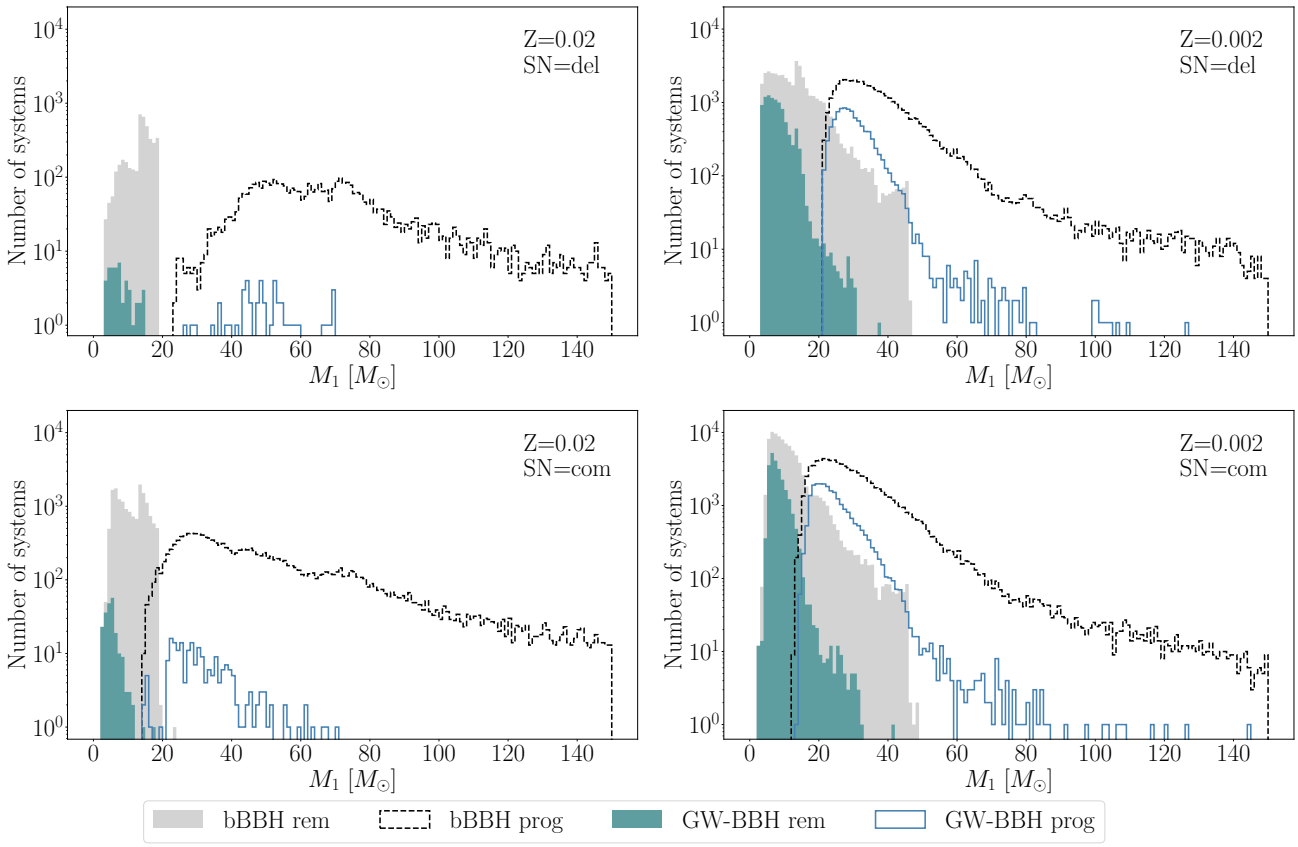

Figure 3. Mass distribution of progenitors (empty histograms) and remnants (filled histograms) primaries in WR-BH systems that formed a bound BBH (grey) and possibly a GW-BBH (green).

case. As we discussed in Figure 2, at such low metallicities the CO core, even if depleted, is still much more massive than the 11 $M_\odot$ threshold below which the production of light black holes is frequent.

We now compare the remnant distributions obtained in Figure 3 with the ones obtained by the single stellar evolution in Figure 1. The binary evolution doesn't modify the maximum BH mass, that is still $\sim$ 20 $M_\odot$ for $Z = 0.02$ and $\sim$ 50 $M_\odot$ for $Z = 0.002$, in agreement with the findings on the single stellar evolution (see Section 3.3). On the contrary, we find that all the remnant distributions in Figure 3 form BHs up to $\sim$ 3 $M_\odot$. Thus, it seems that the $\sim 2-7(10)$ $M_\odot$ mass gap region found in the remnants produced with the compact model can be filled with BHs that evolved in binary systems. By looking at Figure 4 and 5, we see that such low-mass BHs are mainly produced by progenitors with 13 $M_\odot \lesssim M_{\rm ZAMS} \lesssim 20$ $M_\odot$ i.e. progenitors that suffer the most the possibility to explode/implode according to the compactness criterion (in the figures the oscillation appears as a red-patched region).

5.2.1 The impact of the mass transfer

We can explain many of the features of Figure 4 and 5 with the mass transfer episodes. In fact, part of the mass involved in the wind fed, RLO and CE processes is always lost by the system. Less mass retained by the binary means that there is less mass available for the collapse, thus the compact objects are in general lighter than the ones obtained by the single stellar evolution. In particular, the impact of the mass lost by CE processes is bigger on low metallicity stars, that have softer stellar winds and therefore would retain a lot of mass without the removal of the common envelope. Thus, at $Z = 0.002$ we see that most of the remnants in bound BBHs and GW-BBHs have masses lower than the ones expected by the single stellar evolution (up to $\Delta_M \sim 30$ $M_\odot$ difference for $M_{\rm ZAMS} \sim 60$ $M_\odot$). The same effect is visible at $Z = 0.02$, altough the high metallicity systems are less sensible to the mass transfer episodes, so the remnants from the binary evolution are closer to the ones from the isolated evolution (the maximum deviation is of $\Delta_M \sim 10$ $M_\odot$ at $M_{\rm ZAMS} \sim 20$ $M_\odot$).

In the $Z = 0.02$ panels it is more prominent the effect of stable mass transfer, either wind fed or RLO. In particular, for $M_{\rm ZAMS} \gtrsim 30$ $M_\odot$ we see that remnants from the GW-BBHs have primaries less massive and secondaries more massive with respect to the single stellar evolution scenario. On the contrary, both primaries and secondaries remnants from bound BBHs have masses above the isolated scenario for $M_{\rm ZAMS} \gtrsim 30$ $M_\odot$. We recall that it is more likely that the mass is transferred from the primary to the secondary, given that the primary is initially more massive and so it evolves faster. Therefore the secondaries will likely accrete mass and form a BH with more mass than expected from

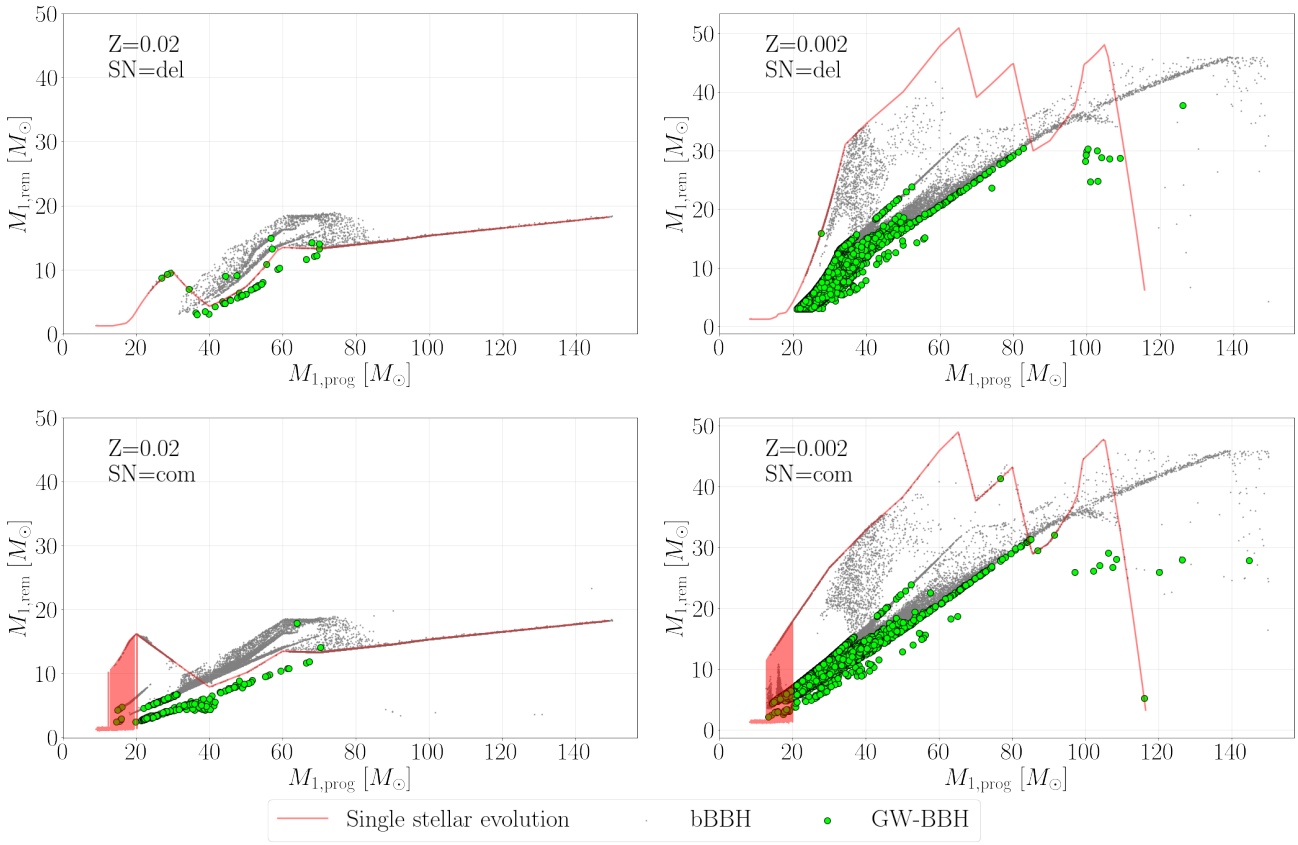

Figure 4. Mass of the remnant M_{rem} as function of the mass of the progenitor M_{prog} for the primaries M_1 of WR-BH systems that formed a bound BBH (small grey dots) and possibily a GW-BBH (big green dots). For comparison we plot in red the expected remnants formed via single stellar evolution as a function of the progenitor mass.

the single stellar evolution. Given the different behaviour of remnants in bound BBHs and GW-BBHs, we can conclude that GW-BBHs systems with $M_{\mathrm{ZAMS}} \gtrsim 30\ M_\odot$ spent significantly more time in stable mass transfer configurations. This conclusion is valid also for the $Z = 0.002$ systems, even though in such binaries the effects of the CE are predominant and mask the range where stable mass transfer is more important.

5.2.2 WR-BHs driven by stellar wind and CE

In Figure 6 we study the mass transfer properties of the WR-BH systems that form GW-BBHs. On the one hand, we characterize the number of CE that each system suffered in its entire evolution. On the other hand, we label each WR-BH system with its Roche Lobe filling parameter R/RL, given by the ratio of the donor radius R and its Roche Lobe radius RL (Eggleton (1983)). We calculate such parameter while the system is in the WR-BH configuration. Following the prescriptions of Hirai & Mandel (2021), we set at $R/RL \geq 0.8$ the threshold to achieve a focused accretion stream on the BH in wind fed systems. We consider WR-BHs below that threshold to be wind fed systems with inefficient mass transfer. On the contrary, we consider an efficient mass transfer episode for WR-BH wind fed systems with $R/RL \geq 0.8$. We also classified systems with $R/RL \geq 1$ i.e. systems with donor that overfilled its RL and entered a RLO episode (whether it is stable or not).

We find that the GW-BBHs remnants distribute almost symmetrically with respect to the bisector that identifies systems with equal masses i.e. mass ratios $q = M_2/M_1 = 1$, in agreement with the literature (see Section 1). It seems that the number of CE is not related to the mass ratio, given that we find GW-BBHs systems with one or two CEs both up and down the $q = 1$ line. Nevertheless, systems with low mass remnants ($M_{1,\mathrm{rem}} \lesssim 13\ M_\odot$ and $M_{2,\mathrm{rem}} \lesssim 13\ M_\odot$) appear to evolve more likely with 2 CE phases, especially if obtained with the compact model and at low metallicity. Although this claim needs to be confirmed with further investigations, it seems in agreement with the discussion carried out in Section 5.2.1.

Systems that experience efficient mass transfers (indicated with a triangle in Figure 6) are very close to the $q = 1$ limit and often above it $q \geq 1$, meaning that the secondary accreted enough mass to form a BH more massive than the one formed by the original primary. If we look at the $Z = 0.002$ panels, that exhibit a larger statistics, we notice that also systems with inefficient mass transfer in the WR-BH phase exhibit $q \geq 1$, meaning that they went through an efficient mass transfer episode at least once in their lifetime (but not during the WR-BH). Nevertheless, we find that binaries that fill their RL more than 80% *during* the WR-BH

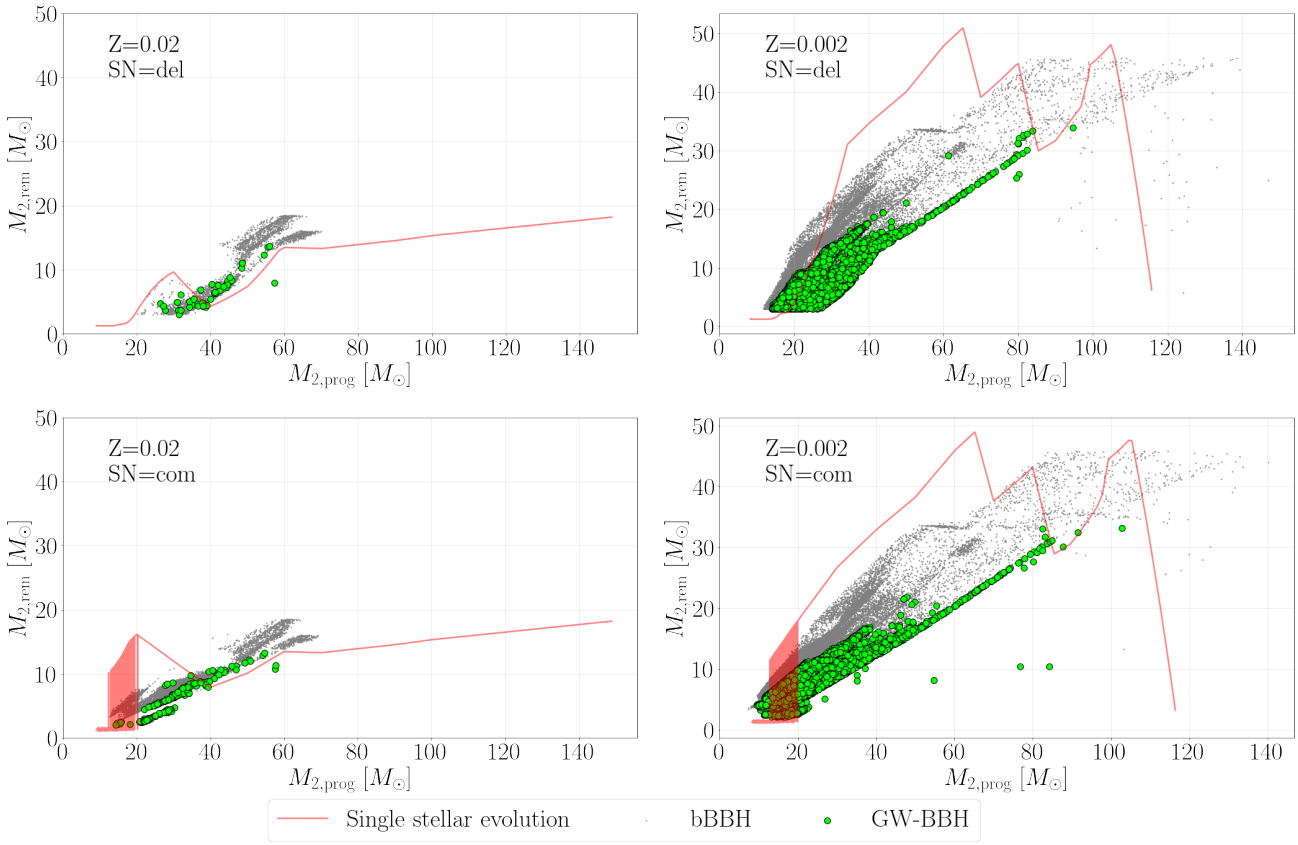

Figure 5. Mass of the remnant $M_{\rm rem}$ as function of the mass of the progenitor $M_{\rm prog}$ for the secondaries M_2 of WR-BH systems that formed a bound BBH (small grey dots) and possibily a GW-BBH (big green dots). For comparison we plot in red the expected remnants formed via single stellar evolution as a function of the progenitor mass.

undergo the most efficient mass transfer episodes, given that they exhibit the higher mass ratios. Moreover, filling the RL at 80% or at 100% seems to make no or little difference in the masses of the remnants.

As showed in Figure 6, only low-mass remnants are able to start an efficient mass transfer during the WR-BH phase. At $Z = 0.002$ we these are remnants with both masses $M_{\rm rem} \lesssim 20\ M_\odot$ while for $Z = 0.002$ the remnants are even lighter, with $M_{\rm rem} \lesssim 13\ M_\odot$. In both cases we expect to form these systems with $M_{\rm prog} \lesssim 60\ M_\odot$.

Finally, we underline that the existence of $q \geq 1$ binaries requires special care when considering the labeling of the masses, especially when comparing the remnants and the progenitors properties (as Fishbach & Kalogera (2021) also pointed out).

5.3 Period distribution

In Figure 7 we report the initial and final periods $\mathcal{P} = \log(P/\text{yrs})$ of WR-BH binaries that formed a bound BBH system and possibly a GW-BBH. We see that for a given metallicity the same range of initial periods produces both bound BBHs and GW-BBHs. For $Z = 0.002$ the useful periods are slightly longer than the ones allowed for $Z = 0.02$, respectively $P \lesssim 800$ and $P \lesssim 200$. In any case we speak of systems wide enough to be sensible to the magnitude of the SN kick. As we discussed in Section 5.2, the more metallic binaries form also the lighter remnants therefore these systems will more likely receive a kick that can possibily unbound the binary. For both metallicities, periods in the range $P_{\rm in} \in [\sim 1\ \text{month}, \sim 10\ \text{yrs}]$ will likely form both a bound BBH and GW-BBH systems.

The final period distribution of the bound BBH binaries seems to be centered at $P_{\rm fin,bBBH} \sim 1$ yr, with shorter periods of $P_{\rm fin,bBBH} \sim 1$ month equally probable only for $Z = 0.002$. Lower final periods can be reached more easily in low metallicity systems, that retain a lot of mass and lose it only in the CE events. According to the $\alpha\lambda$ prescription implemented in SEVN2 (see Section 3.4), it is more likely to survive to the CE and avoid the merging if the system is able to expell a massive envelope, which seems exactly the case of the low metallicity systems. The same reasoning can be used to explain the large number of $Z = 0.002$ systems that form a GW-BBH merging, even though the original bound BBH population was already larger than the one at $Z = 0.02$.

The distribution of the periods of the GW-BBHs is peaked at about $P_{\rm fin,GW-BBH} \sim 1$ day and has an asymmetric tail that allows periods up to $P_{\rm fin,GW-BBH} \sim 1$ hour. Shorter periods would result in a merging before the formation of a BBH system, for instance because of a collision. On the other hand, periods much larger than $P_{\rm fin,GW-BBH} \sim$

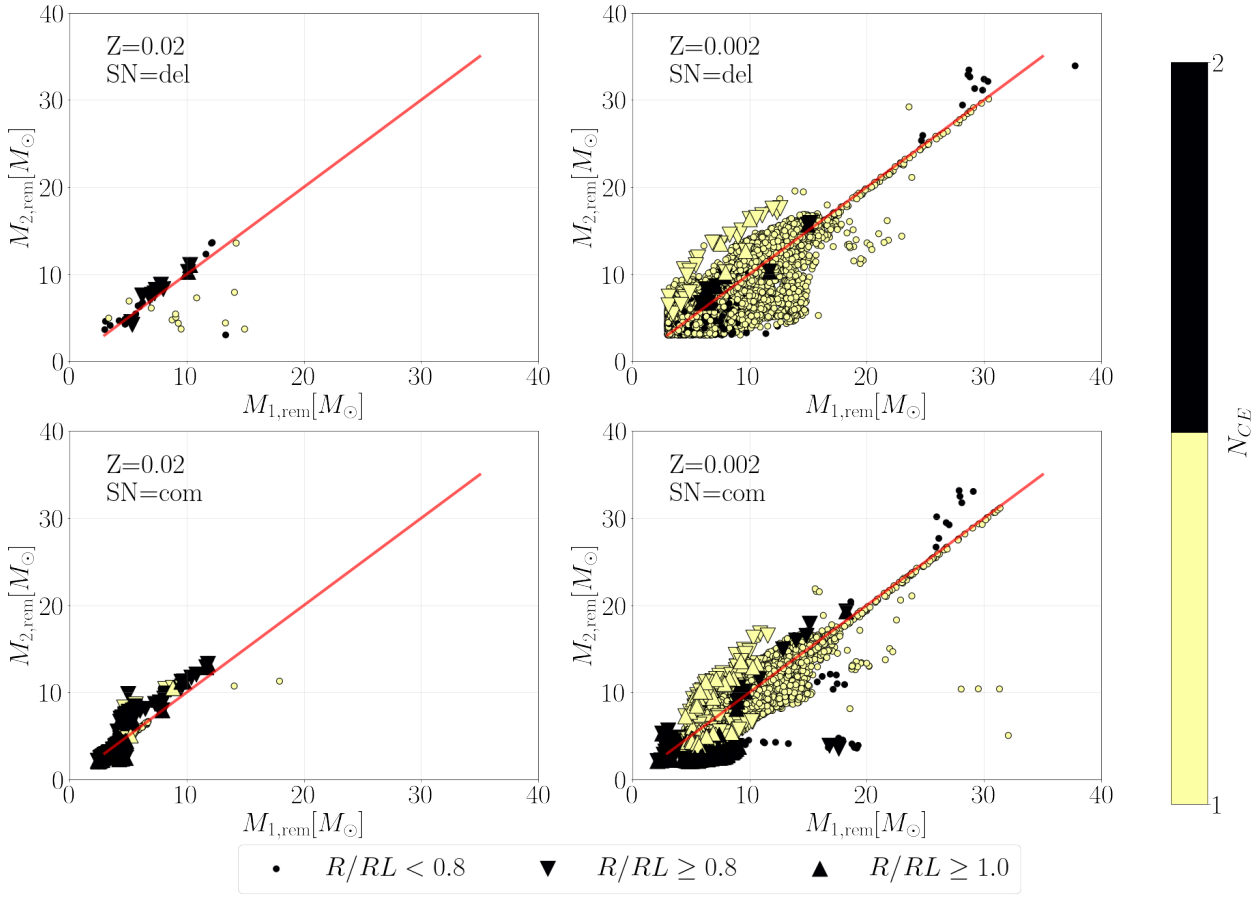

Figure 6. Masses of the remnants of all the WR-BH systems that formed a GW-BBH. For reference, we indicated in red the line corresponding to equal masses $q = M_2/M_1 = 1$. The circle indicates systems with stars that never filled their Roche Lobes more than 80% while in the WR-BH phase. The down-triangle and up-triangle mark systems that during the WR-BH configuration filled their Roche Lobes respectively more than 80% (wind fed) and 100% (RLO or CE). The color of the points indicates the number of CE events that occured in the entire life of the binary.

1 day could be too large to merge via GW emission within a Hubble time. Nevertheless, some systems simulated with the delayed model exhibit few GW-merging also with periodS of $P_{\rm fin,GW-BBH} \sim 1$ month; it could be either a feature of the delayed model or a particular combination of the masses and orbital parameters. For the moment we don't consider reliable this upper limit and we leave the problem open to further investigations.

6 CONCLUSIONS

We explored the $Z = 0.02$ and $Z = 0.002$ metallicities to estimate upper and lower boundaries in the formation of GW-BBHs from WR-BH systems that could be observed in the nearby universe. We simulated $\sim 10^6$ binaries for each metallicity with two SN models, delayed and compact, to remove possible biases. We are therefore confident that the following results are general:

- More than $\sim 90\%$ of all the GW-BBH systems are generated from binaries that experienced the WR-BH configuration.
- WR-BH systems constitute only $\sim 1-4\%$ of all the binaries at $Z = 0.02$ and $\sim 8-16\%$ of the binaries at $Z = 0.002$.
- Once the WR-BH systems are formed, only $\sim 50\%$ of them will form a BBH.
- BBHs from WR-BHs are usually bound BHs but only $\sim 25\%$ of the bound BBH binaries produces a GW-BBHs at $Z = 0.002$. If $Z = 0.02$, the percentage reduces to $\sim 1\%$.
- Only $\sim 14-19\%$ of the WR-BH systems at $Z = 0.002$ host a star that fills its Roche Lobe more than 80% while in the WR-BH configuration. At $Z = 0.02$ only $\sim 5-21\%$ of the systems fulfill this condition. It means than about $\sim 24-59\%$ of the GW-BBHs forming from WR-BHs at $Z = 0.02$ come from systems that we expect to shine as BH-XRBs. For $Z = 0.002$ this percentage is almost negligible: $\sim 0.4-7\%$.
- Low metallicities ($Z = 0.002$) favour the formation of WR-BH systems, that possibly form GW-BBHs. Stars with $20\ M_\odot \lesssim M_{\rm ZAMS} \lesssim 80\ M_\odot$ form GW-BBH systems with

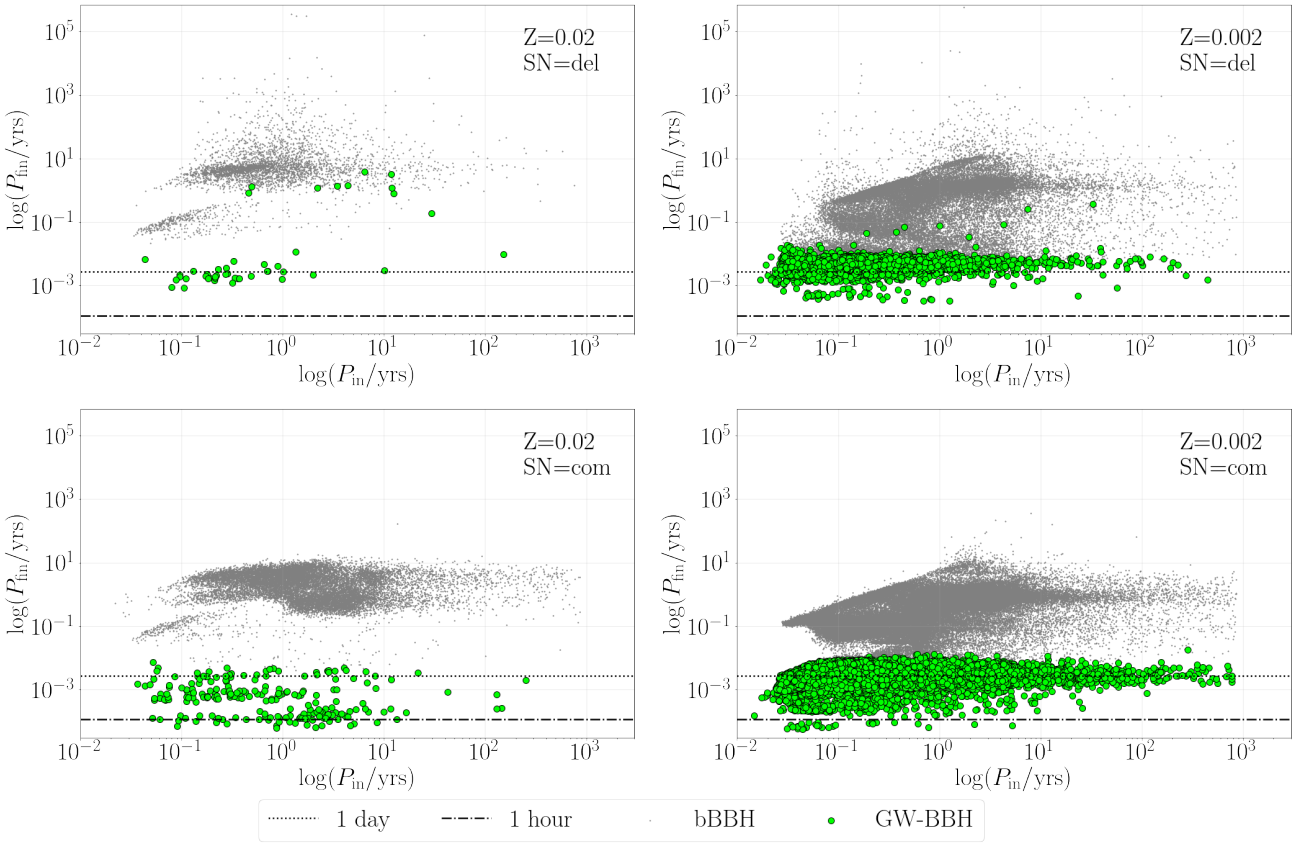

Figure 7. Initial and final period $\mathcal{P} = \log(P/\mathrm{yrs})$ in WR-BH systems that formed a bound BBH (small grey dots) and possibly a GW-BBH (big green dots). For reference, we indicated the $P = 1$ day threshold with a black dotted line and the $P = 1$ hour threshold with the black dash-dotted line.

remnants $3\ M_\odot \lesssim M_{\rm rem} \lesssim 30\ M_\odot$. Their evolution is dominated by CE episodes. The subset of $3\ M_\odot \lesssim M_{\rm rem} \lesssim 20\ M_\odot$ is the one affected the most by efficient mass transfer in the WR-BH configuration.

- High metallicities ($Z = 0.02$) disfavour the formation of WR-BH systems, that possibly form GW-BBHs. Stars with $20\ M_\odot \lesssim M_{\rm ZAMS} \lesssim 60\ M_\odot$ form GW-BBH systems with remnants $3\ M_\odot \lesssim M_{\rm rem} \lesssim 20\ M_\odot$. A subset of them, with $3\ M_\odot \lesssim M_{\rm rem} \lesssim 13\ M_\odot$, is more likely to experience efficient mass transfer episodes in the WR-BH configuration and suffer two CEs.
- The period distribution of the GW-BBHs is narrowly peaked at $P_{\rm fin,GW-BBH} \sim 1$ day with an asymmetry up to $P_{\rm fin,GW-BBH} \sim 1$ hour. The period of the progenitor systems is $P_{\rm in} \in [1\ \mathrm{month}, 10\ \mathrm{yrs}]$.
- The isolated binary evolution channel favours the formation of equal-mass remnants $q = M_2/M_1 = 1$.

We also point out that the delayed model is probably not the best-suited CCSN model to analyze WR-BH systems because it:

- produces BHs only from stars with $M_{\rm ZAMS} \gtrsim 20\ M_\odot$. This is probably the cause of the sistematic low number of WR-BHs formed at both metallicities. In fact, the compact model produces sistematically more systems in the metallicities explored.

- the BH distribution monotonically depends on the growth of the CO core. For WR stars, that exhibit progressively the innermost layers, this is an undesiderable feature.

We conclude discussing the fate of the seven WR-BH candidates. We will adopt the informations obtained from the simulations and discard the information on the masses measured in the candidates. The observed WR-BH have metallicities of $Z \sim 0.002$ and periods of $\sim 1 - 100$ hours, close both to the lower and upper boundary for the final periods of GW-BBHs. With the formation of a binary compact object we expect that the orbiting masses reduce. Thus, their period should slightly increase (third Kepler law), entering in a region where they might not merge within a Hubble time (as the M101 ULX X-1 system discussed in the text). Nevertheless, with these information we are confident that none of the systems will collide or merge via mechanisms different than the GW decay.

References

Abbott B. P., Abbott R., Abbott T. D., et al. 2016, Phys. Rev. Lett., 116, 061102
Abbott R., Abbott T. D., et al. 2021a, Physical Review X, 11, 021053

Abbott R., Abbott T. D., Abraham S., et al. 2021b, ApJ, 913, L7
Alsing J., Silva H. O., Berti E., 2018, MNRAS, 478, 1377
Binder B. A., et al., 2021, The Astrophysical Journal, 910, 74
Bondi H., Hoyle F., 1944, Monthly Notices of the Royal Astronomical Society, 104, 273
Chen Y., Bressan A., Girardi L., Marigo P., Kong X., Lanza A., 2015, MNRAS, 452, 1068
Claeys J. S. W., Pols O. R., Izzard R. G., Vink J., Verbunt F. W. M., 2014, A&A, 563, A83
Clark J. S., Crowther P. A., 2004, A&A, 414, L45
Crowther P. A., Barnard R., Carpano S., Clark J. S., Dhillon V. S., Pollock A. M. T., 2010, Monthly Notices of the Royal Astronomical Society: Letters, 403, L41
Eggleton P. P., 1983, ApJ, 268, 368
Esposito P., Israel G. L., Sidoli L., Mapelli M., Zampieri L., Motta S. E., 2013, Monthly Notices of the Royal Astronomical Society, 436, 3380
Esposito P., Israel G. L., Milisavljevic D., Mapelli M., Zampieri L., Sidoli L., Fabbiano G., Rodríguez Castillo G. A., 2015, MNRAS, 452, 1112
Fishbach M., Kalogera V., 2021, arXiv e-prints, p. arXiv:2111.02935
Fryer C. L., Belczynski K., Wiktorowicz G., Dominik M., Kalogera V., Holz D. E., 2012, ApJ, 749, 91
Giacobbo N., Mapelli M., Spera M., 2018, MNRAS, 474, 2959
Gräfener G., Hamann W. R., 2008, A&A, 482, 945
Hertz P., Joss P., Rappaport S., 1978, The Astrophysical Journal, 224, 614
Hirai R., Mandel I., 2021, Publ. Astron. Soc. Australia, 38, e056
Hobbs G., Lorimer D. R., Lyne A. G., Kramer M., 2005, MNRAS, 360, 974
Humphreys R. M., Davidson K., 1979, The Astrophysical Journal, 232, 409
Hurley J. R., Tout C. A., Pols O. R., 2002, MNRAS, 329, 897
Kalogera V., 2000, ApJ, 541, 319
Kalogera V., Baym G., 1996, ApJ, 470, L61
Kroupa P., 2001, Monthly Notices of the Royal Astronomical Society, 322, 231
Laycock S. G. T., Maccarone T. J., Christodoulou D. M., 2015, MNRAS, 452, L31
Limongi M., Chieffi A., 2010, in Journal of Physics Conference Series. p. 012002, doi:10.1088/1742-6596/202/1/012002
Liu J.-F., Bregman J. N., Bai Y., Justham S., Crowther P., 2013, Nature, 503, 500
Maccarone T. J., Lehmer B. D., Leyder J. C., Antoniou V., Hornschemeier A., Ptak A., Wik D., Zezas A., 2014, MNRAS, 439, 3064
Mapelli M., Ripamonti E., Zampieri L., Colpi M., Bressan A., 2010, Monthly Notices of the Royal Astronomical Society, 408, 234
Mapelli M., Spera M., Montanari E., Limongi M., Chieffi A., Giacobbo N., Bressan A., Bouffanais Y., 2020, ApJ, 888, 76
Moe M., Di Stefano R., 2017, The Astrophysical Journal Supplement Series, 230, 15
Nugis T., Lamers H. J. G. L. M., 2000, A&A, 360, 227
O'Connor E., Ott C. D., 2011, ApJ, 730, 70
Özel F., Psaltis D., Narayan R., McClintock J. E., 2010, The Astrophysical Journal, 725, 1918
Patton R. A., Sukhbold T., 2020, MNRAS, 499, 2803
Peters P. C., 1964, Physical Review, 136, B1224
Rastello S., Mapelli M., Di Carlo U. N., Iorio G., Ballone A., Giacobbo N., Santoliquido F., Torniamenti S., 2021, MNRAS, 507, 3612
Rodriguez C. L., Zevin M., Pankow C., Kalogera V., Rasio F. A., 2016, ApJ, 832, L2
Sana H., et al., 2012, Science, 337, 444
Silverman J. M., Filippenko A. V., 2008, The Astrophysical Journal, 678, L17
Spera M., Mapelli M., 2017, MNRAS, 470, 4739
Spera M., Mapelli M., Bressan A., 2015, MNRAS, 451, 4086
Spera M., Mapelli M., Giacobbo N., Trani A. A., Bressan A., Costa G., 2019, MNRAS, 485, 889
Sukhbold T., Woosley S. E., 2014, ApJ, 783, 10
Sukhbold T., Ertl T., Woosley S. E., Brown J. M., Janka H. T., 2016, ApJ, 821, 38
The LIGO Scientific Collaboration et al. 2021, arXiv e-prints, p. arXiv:2111.03606
Thompson T. A., et al., 2019, Science, 366, 637
Tutukov A. V., Fedorova A. V., Cherepashchuk A. M., 2013, Astronomy Reports, 57, 657
Webbink R. F., 1984, ApJ, 277, 355
Webbink R. F., 1985, Stellar evolution and binaries. p. 39
Wyrzykowski Ł., Mandel I., 2020, A&A, 636, A20
Zdziarski A. A., Misra R., Gierliński M., 2010, Monthly Notices of the Royal Astronomical Society, 402, 767
Zdziarski A. A., Mikolajewska J., Belczynski K., 2013, MNRAS, 429, L104
van Kerkwijk M. H., Geballe T. R., King D. L., van der Klis M., van Paradijs J., 1996, A&A, 314, 521